Received: 20 August 2021 | Revised: 29 October 2021 | Accepted: 8 November 2021

DOI: 10.1096/fj.202101334R

THE FASEB JOURNAL

RESEARCH ARTICLE

Soluble very low-density lipoprotein receptor (sVLDLR) inhibits fibrosis in neovascular age-related macular degeneration

Xiang Ma | **Yusuke Takahashi** | **Wenjing Wu** | **Jianglei Chen** | **Marcus Dehdarani** | **Wentao Liang** | **Young-Hwa Shin** | **Siribhinya Benyajati** | **Jian-xing Ma**

Department of Physiology, University of Oklahoma Health Sciences Center, Oklahoma City, Oklahoma, USA

Correspondence
Jian-xing Ma, Department of Physiology, University of Oklahoma Health Sciences Center, BSEB 328B, 941 Stanton L. Young Blvd, Oklahoma City, OK 73104, USA.
Email: jian-xing-ma@ouhsc.edu

Funding information
National Institutes of Health (NIH), Grant/Award Number: EY019309, EY012231, EY028949, EY032930 and EY032931; Diabetic Animal Core and Histology and Image Core of diabetic COBRE, Grant/Award Number: GM122744; NEI P30, Grant/Award Number: EY021725

Abstract

Subretinal fibrosis is a key pathological feature in neovascular age-related macular degeneration (nAMD). Previously, we identified soluble very low-density lipoprotein receptor (sVLDLR) as an endogenous Wnt signaling inhibitor. This study investigates whether sVLDLR plays an anti-fibrogenic role in nAMD models, including *Vldlr*$^{-/-}$ mice and laser-induced choroidal neovascularization (CNV). We found that fibrosis factors including P-Smad2/3, α-SMA, and CTGF were upregulated in the subretinal area of *Vldlr*$^{-/-}$ mice and the laser-induced CNV model. The antibody blocking Wnt co-receptor LRP6 significantly attenuated the overexpression of fibrotic factors in these two models. Moreover, there was a significant reduction of sVLDLR in the interphotoreceptor matrix (IPM) in the laser-induced CNV model. A transgenic strain (*sVLDLR-Tg*) with sVLDLR overexpression in the IPM was generated. Overexpression of sVLDLR ameliorated the profibrotic changes in the subretinal area of the laser-induced CNV model. In addition, Wnt and TGF-β signaling synergistically promoted fibrogenesis in human primary retinal pigment epithelium (RPE) cells. CRISPR/Cas9-mediated *LRP6* gene knockout (KO) attenuated this synergistic effect. The disruption of VLDLR expression promoted, while the overexpression of sVLDLR inhibited TGF-β-induced fibrosis. These findings suggest that overactivated Wnt signaling enhances the TGF-β pathway in subretinal fibrosis. sVLDLR confers an antifibrotic effect, at least partially, through the inhibition of Wnt signaling and thus, has therapeutic potential for fibrosis.

KEYWORDS

fibrosis, macular degeneration, TGF-β signaling pathway, very low-density lipoprotein receptor, Wnt signaling pathway

Abbreviations: ARPE-19, a human retinal pigment epithelial cell line; CNV, choroidal neovascularization; CTGF, connective tissue growth factor; IPM, interphotoreceptor matrix; LRP, low-density lipoprotein receptor-related protein; nAMD, neovascular age-related macular degeneration; ONL, outer nuclear layer; RPE, retinal pigment epithelium; sVLDLR, soluble very low-density lipoprotein receptor; sVLDLR-Tg, a transgenic mouse strain with sVLDLR overexpression; TCF, T-cell factor; VEGF, vascular endothelial growth factor; VLDLR, very low-density lipoprotein receptor; WCM, Wnt3A conditioned medium.

1 | INTRODUCTION

Age-related macular degeneration (AMD) is the leading cause of irreversible blindness in the elderly worldwide.[1-3] In neovascular AMD (nAMD), new vessels grow from the choroid, break through the Bruch's membrane and RPE, and intrude the neural retina.[1] Choroidal neovascularization (CNV) often results in hemorrhage and exudative changes, and with time, promotes the development of subretinal fibrosis.[4] Subretinal space, by definition, refers to tissues beneath the retina, including the retinal pigment epithelium (RPE), Bruch's membrane, choroid, and the extracellular matrix between the retina and RPE (termed as the interphotoreceptor matrix, IPM). The IPM plays a crucial role in the intercellular communication between the RPE and the retina and maintains retinal function and homeostasis.[5] The accumulation of excessive fibrous connective tissues and the substantial remodeling of the extracellular matrix (ECM) in the subretinal space is often the primary cause of irreversible vision loss in patients with advanced nAMD. Although anti-VEGF therapies are highly effective for inhibiting pathological angiogenesis and ameliorating vascular leakage in nAMD, approximately 10% to 30% of nAMD patients do not respond to the anti-VEGF treatment.[6] Moreover, recent studies reported that anti-VEGF therapy might cause the development of subretinal fibrosis.[2,7] There is no effective treatment for subretinal fibrosis in nAMD. Therefore, the untreatable subretinal fibrosis in advanced nAMD represents a pressing medical challenge.

The canonical Wnt signaling profoundly affects many physiological and pathological processes, including angiogenesis and fibrosis.[8–10] Accumulating evidence demonstrates that canonical Wnt signaling is overactivated in fibrotic diseases, which promotes TGF-β-mediated fibrosis.[11] The canonical Wnt signaling is activated upon the binding of the Wnt ligand to the Wnt co-receptor complex consisting of frizzled receptors and low-density lipoprotein receptor-related protein 5 or 6 (LRP5/6).[12,13] It results in the phosphorylation of LRP5/6 and the dissociation of the kinase complex containing GSK-3β, leading to decreased phosphorylation and degradation of cytoplasmic β-catenin.[14] Then, non-phosphorylated β-catenin is stabilized and translocates into the nucleus and associates with T-cell factor (TCF) to activate the expression of Wnt target genes, including pro-angiogenic factors, such as vascular endothelial growth factor (VEGF), and profibrotic factors, such as connective tissue growth factor (CTGF). Our previous studies demonstrated that Wnt signaling is overactivated in macular tissues of patients with nAMD.[15] The aberrant activation of Wnt signaling has been found in the RPE-choroid complex of *Vldlr*$^{-/-}$ mice and the laser-induced CNV model, two classical animal models of nAMD.[16,17] The inhibition of canonical Wnt signaling by a Wnt receptor-blocking antibody (Mab2F1) alleviated vascular leakage and pathological angiogenesis in both nAMD models.[16] However, it remains unknown if blockade of LRP6 also confers an antifibrotic effect in nAMD models.

Canonical Wnt signaling is closely regulated by endogenous inhibitors, such as kallistatin, dickkopf-1, and very low-density lipoprotein receptor (VLDLR).[18] A growing body of evidence indicates that VLDLR plays a crucial role in AMD pathogenesis among these natural inhibitors. VLDLR genetic variants are associated with AMD incidence in human studies.[19] Moreover, *Vldlr*$^{-/-}$ mice demonstrated a broad spectrum of nAMD-like phenotypes, including retinal inflammation, retinal vascular leakage, CNV, and progressive ERG decline.[17,20] VLDLR is a multifunctional integral membrane protein that belongs to the low-density lipoprotein receptor gene family.[21] It was initially recognized to mediate VLDL binding and lipid transport.[22,23] Recently, we demonstrated that VLDLR sheds its soluble extracellular domain, soluble VLDLR (sVLDLR), to function as an endogenous inhibitor of Wnt signaling by binding with LRP6.[24,25] Considering that canonical Wnt signaling is overactivated in the subretinal space of the laser-induced CNV model, the present study investigated if laser-induced CNV results in reduced sVLDLR levels in the IPM, contributing to the aberrant activation of Wnt signaling. Of particular interest, this study addressed the question of whether overexpressed sVLDLR in the IPM rescues the subretinal fibrosis of the laser-induced CNV model. In this study, we also investigated the antifibrotic effect of sVLDLR in mouse and human RPE cells.

2 | MATERIALS AND METHODS

2.1 | Animals

Vldlr gene knockout (*Vldlr*$^{-/-}$) mice on the C57BL/6J background were purchased from Jackson Laboratories (Bar Harbor, ME, USA). All mice were housed in a specific pathogen-free (SPF) environment at 25°C under a 12/12 h light/dark cycle in the animal facility of the University of Oklahoma Health Sciences Center (OUHSC). In all procedures, mice were anesthetized with an intraperitoneal injection of the ketamine-xylazine mix (k, 100 mg/kg; x, 5 mg/kg). The pupils were dilated with topical application of cyclopentolate (Akorn, Lake Forest, IL, USA). Mice were cared for in compliance with the guidelines of the ARVO Statement for the Use of Animals in Ophthalmic and Visual Research, and all studies were conducted following the

protocol approved by the Institute Animal Care and Use Committee (IACUC) at OUHSC.

The transgenic mice that overexpressed the human VLDLR ectodomain in the photoreceptors (*sVLDLR-Tg*) were generated. The rhodopsin promoter and the sequence encoding the human VLDLR ectodomain were cloned into a Tet-on inducible gene expression vector (VectorBuilder, Chicago, IL, USA) (Figure S1A). The transgene vector was microinjected into the embryo of C57BL/6J background through a contracted service with Texas A&M Institute for Genomic Medicine (College Station, TX, USA). Transgenic founders were identified by genotyping with PCR using a forward primer (5′-GAGCGTCAGCAGGCAGCATA-3′) and a reverse primer (5′-TCTGCGGAACAACGCCAAGT-3′). The PCR conditions were 95°C for 12 min, followed by 35 cycles of 94°C for 30 seconds, 61°C for 30 seconds, and 72°C for 1 min. For inducing sVLDLR expression, 3-week-old *sVLDLR-Tg* mice were fed with water containing 2 mg/ml doxycycline ad libitum for 3 weeks. WT littermates were also subjected to doxycycline treatment with the same dose and duration. Five-week-old *sVLDLR-Tg* mice and WT littermates were used for the laser-induced CNV model.

2.2 | Cell culture

The human retinal pigment epithelial cell (ARPE-19) was purchased from ATCC (Manassas, VA, USA) and cultured in DMEM/F12 medium containing 10% fetal bovine serum (FBS) and 1% Penicillin/Streptomycin. ARPE-19 cells with *LRP6* knockout (KO) by CRISPR/Cas9 technology were maintained under the same conditions.[18] Primary cultures of mouse RPE cells were performed according to established protocols described previously. Briefly, eyeballs were harvested from 4 to 6-week-old mice. The connective tissues were carefully removed from eyeballs with sterile ophthalmic scissors and forceps. The eyeballs were incubated in a pre-warmed serum-free growth medium containing 2% dispase II for 45 min at 37°C. Then, they were washed twice in a serum-containing growth medium, and the RPE-choroid-sclera complexes (eyecups) were gently dissected from the eyeballs. The RPE sheets were then gently peeled off from the eyecups under the dissecting microscope and maintained in the culture medium supplemented with 10% FBS, N1 supplement (1X), MEM non-essential amino acid (1X), 2 mM L-glutamine, 250 μg/ml Taurine, 20 ng/ml hydrocortisone, 10 ng/ml triiodothyronine, and 1% penicillin/streptomycin.

Transduction and preparation of conditioned medium were described previously.[24,25] For the transduction, adenovirus expressing sVLDLR and adenovirus expressing red fluorescent protein (RFP, dsRed) were prepared in house. Briefly, the coding region of human VLDLR ectodomain and dsRed were separately subcloned into pShuttle-CMV vectors. According to published protocols, the generation of recombinant adenovirus genomic DNA, packaging, amplification, and titration were carried out as described previously.[26,27] ARPE-19 cells were infected with adenovirus at a multiplicity of infection (MOI) of 50 for 48 h. For the preparation of conditioned medium, L cells expressing biologically active Wnt3A (W cells) and control L cells were purchased from ATCC (Manassas, VA, USA) and cultured in DMEM containing 10% FBS. Two days after L and W cells reached 100% confluence, the conditioned medium from L cells and W cells were harvested as LCM and WCM, respectively.

2.3 | Mab2F1 purification

The hybridoma cell line secreting Mab2F1 was generated as described previously.[28] The purification process was shown in Figure S2. The hybridoma cells were cultured in RPMI1640 media containing 20% FBS. After cells expanded to 4 T175 flasks, the hybridoma cells were cultured in serum-free CD hybridoma media for three days. The media were collected, adjusted pH to 7.4, and filtered through the 0.22-μm filter. Then, the media were applied to an equilibrated Protein G column at a 2 ml/min flow rate. After that, the Protein G column was washed with 10 ml PBS. The bound Mab2F1 was eluted using 0.1 M glycine (pH 2.5). The elution was neutralized with 1 M Tris-base (pH 9.0). The protein bands in each elution fraction were detected by Coomassie blue staining. The Mab2F1 in neutralized elution buffer was dialyzed against normal saline at 4°C and then was stored in −80°C until use.

2.4 | Luciferase reporter assay

Luciferase-based reporter assay was performed to measure TCF/β-catenin activity in ARPE-19 cells as described previously.[29] Briefly, ARPE-19 cells were cultured in 24-well plates and transfected with 0.30 μg TOPFLASH vector containing the luciferase reporter gene under the control of a promoter containing β-catenin/TCF-binding sites and co-transfected with 0.20 μg pRL-TK plasmid in each well using lipofectamine 2000 (ThermoFisher, Carlsbad, CA, USA). The TCF/β-catenin activity was detected and normalized to Renilla luciferase readout using the luciferase reporter system (Promega, Medison, WI, USA). Wnt3A conditioned media were harvested from L cells stably expressing human Wnt3A (ATCC, Manassas, VA).

2.5 | Laser-induced choroidal neovascularization (CNV)

CNV was induced in 2-month-old mice using the image-guided laser induction system (Micron IV, Phoenix Research Laboratories, Pleasanton, CA, USA) as described previously.[30,31] After mice were anesthetized and pupils were dilated, four laser burns per eye around the optic nerve were generated in the subretinal space. Laser induction was set up with a wavelength of 532 nm, a spot diameter of 50 μm, a duration of 100 ms, and a laser power of 240 mW. The eyes were excluded if (1) the areas of hemorrhages were larger than 2-fold of the lesion diameter and (2) two or more than two shots caused the haze lesion, instead of the bubble formation. The bubble formation right after the laser induction indicated the successful laser shot with Bruch's membrane rupture. For measuring the fibrosis markers in the subretinal area of the laser-induced CNV model, the RPE-choroid complexes were harvested for Western blot analysis or immunostaining at indicated time points.

2.6 | Intravitreal injection

After mice were anesthetized and pupils were dilated, an incision with an approximate length of 0.5 mm was created in the sclera posterior to the limbus with a blade. A 33-gauge needle attached to a Nanofil syringe (World Precision Instruments, Sarasota, FL, USA) was then penetrated through the incision to deliver 1.5 μl of Mab2F1 (4 mg/ml in normal saline solution) or the same dose of nonspecific mouse IgG into the vitreous cavity. Ultra-micro-pump III (World Precision Instruments) was used to control the injection speed at 0.5 μl/sec. After the injection, one drop of antibiotic ointment was applied to the cornea and sclera.

2.7 | Fundus fluorescein angiography

WT and *sVLDLR-Tg* mice were anesthetized, and pupils were dilated, as mentioned above. Mice were intraperitoneally injected with 5% sodium fluorescein (Sigma-Aldrich, St. Louis, MO, USA) at a dose of 20 μl per 10 g of mouse body weight. Fluorescent fundus images were captured at 5 min after the fluorescein injection using a retinal imaging microscope, Micron IV (Phoenix Research Laboratories, Pleasanton, CA, USA). The vascular leakage was quantified by measuring the areas of fluorescein leakage at the laser spots using Image J software (Bethesda, MD, USA).

2.8 | Immunofluorescent staining and analysis

The eyeballs were harvested and fixed in 4% paraformaldehyde in phosphate-buffered saline (PBS) for 1 h. The eyecups were isolated and flat-mounted. For the cryosection, the eyeballs were embedded in the OCT compound. Then, the flat-mounted tissues and frozen section slides were blocked in 5% BSA with 0.2% Triton-X100 for 1 h. Then, the slides were incubated with primary antibodies overnight at 4°C. After three washes with PBS, slides were incubated with a secondary antibody for 2 h. The slides were mounted with the mounting buffer and then photographed with a laser scanning confocal microscope (FV1000) (Olympus, PA, USA). The areas of fibrosis markers at laser spots were measured using Image J software.

2.9 | Western blot analysis

Western blot analysis was performed as described previously.[31,32] For measuring proteins from the RPE sheets, the eyecups were incubated in 0.25 M EDTA buffer in a 37°C incubator for 30 min.[33] Then, the RPE sheets were peeled off from the eyecups. RPE sheets were pooled from 1 mouse for the preparation of each sample. The RPE tissues were homogenized by ultrasonic disruption. For measuring sVLDLR in the IPM of laser-induced CNV, the IPM were collected from 5 mice (10 eyeballs) per group and combined according to a documented protocol.[25,34] Briefly, the retinas were collected and gently rinsed with PBS containing proteinase inhibitors. The PBS was then centrifuged at 1000× *g* for 5 min to remove cell debris, followed by ultra-centrifugation at 70 000× *g* for 1 h to remove cell membranes. The supernatant was collected as the IPM. β-Actin was used as a loading control. If α-SMA was the target protein, GAPDH was used as a loading control. Primary and secondary antibodies used in this study are shown in Table S1.

2.10 | Statistical analysis

At least three independent measurements were conducted for each in vitro assay, and at least six mice per group were used for animal experiments. All values were presented as mean ± standard error of the mean (SEM). Statistical analyses were performed using a 2-tailed Student's *t*-test to compare two groups, or ANOVA followed by the Student–Newman–Keuls test when more than two groups were compared. A p value of $< .05$ was considered statistically significant.

3 | RESULTS

3.1 | Overactivated TGF-β/Smad signaling and fibrosis were present in the retinas and the subretinal region of *Vldlr*$^{-/-}$ mice

As the TGF-β/Smad pathway is known to play a crucial role in fibrosis,[35] we measured the total Smad2/3 and phosphorylated Smad2/3 (P-Smad2/3), and its downstream profibrotic markers, including α-SMA and CTGF using Western blot analysis. Protein levels of phosphorylated Smad2/3 (P-Smad2/3) were significantly increased in the RPE of 3-month-old *Vldlr*$^{-/-}$ mice compared to those in WT littermates (Figure 1A–C). Protein levels of CTGF and α-SMA were significantly increased in the RPE of *Vldlr*$^{-/-}$ mice compared to those of the WT littermates (Figure 1D–F). Moreover, immunostaining showed enhanced α-SMA signaling in the RPE layer of *Vldlr*$^{-/-}$ mice relative to the control group, indicating the RPE acquisition of myofibroblast-like phenotype in *Vldlr*$^{-/-}$ mice (Figure 1G). There was also increased α-SMA immunostaining in the CNV areas of *Vldlr*$^{-/-}$ mice (Figure 1G). Taken together, these results demonstrated that *Vldlr* KO resulted in increased TGF-β/Smad signaling and profibrotic changes in the subretinal region.

3.2 | Blockade of Wnt signaling inhibited subretinal fibrosis in *Vldlr*$^{-/-}$ mice

Mab2F1 is a monoclonal antibody specifically recognizing and blocking the Wnt co-receptor, LRP6.[28] It has shown the inhibitory effect on canonical Wnt signaling and subsequent pathological angiogenesis and vascular leakage in animal models.[16,28] However, it remains unclear if Mab2F1 has an antifibrotic effect. In this study, Mab2F1 was purified following a documented protocol.[28] The Coomassie blue staining of different elution fractions of Mab2F1 was shown in Figure S2B. The luciferase-based assay showed that Mab2F1 inhibited Wnt3A conditioned medium (WCM)-induced TCF/β-catenin activity (Figure S2C). To evaluate the antifibrotic effect of Mab2F1, the isolated RPE sheets were harvested from 3-month-old *Vldlr*$^{-/-}$ mice at day 7 post-intravitreal injection of Mab2F1 or nonspecific mouse IgG as control. Protein levels of P-Smad2/3, CTGF, and α-SMA in the isolated RPE sheets were significantly reduced in Mab2F1-treated *Vldlr*$^{-/-}$ mice relative to those in IgG-treated mice (Figure 2A–F). Total Smad2/3 levels remained unchanged between the two groups (Figure 2A,C). As shown by immunostaining, Mab2F1 treatment alleviated the increase of α-SMA in the RPE layer of *Vldlr*$^{-/-}$ mice (Figure 2G). These results indicated that disruption of canonical Wnt signaling by blocking LRP6 inhibited the subretinal fibrosis in *Vldlr*$^{-/-}$ mice.

3.3 | Reduced sVLDLR levels in the IPM and subretinal fibrosis were present in the laser-induced CNV model

Previous studies showed that laser elicited subretinal fibrotic changes at various days post laser shot.[37,38] To better understand the dynamic change of the profibrotic pathway and markers, we selected 3, 7, and 21 days post-laser as time points for measurements. As shown in Figure 3A–F, protein levels of P-Smad2/3, CTGF, and α-SMA were significantly increased at day 3 and reached the peak level at day 7 and then decreased toward the baseline at day 21 post laser induction. Total Smad2/3 levels remained unchanged in the laser-treated group compared to non-laser controls (Figure 3A,C). Importantly, we measured sVLDLR in the IPM and the full-length VLDLR in the retina. sVLDLR levels in the IPM were significantly reduced, whereas the full-length VLDLR in the retina showed no significant difference in the laser-induced CNV model relative to the non-laser group, indicating that the shedding of sVLDLR into the IPM was reduced in the laser-induced subretinal fibrosis model (Figure 3G–I).

3.4 | Mab2F1 alleviated subretinal fibrosis of the laser-induced CNV model

Two days post-laser induction, Mab2F1 was intravitreally injected, with mouse IgG as control. Five days post-injection, the RPE was harvested for measurements. Mab2F1 treatment significantly reduced levels of P-Smad2/3, CTGF, and α-SMA compared to the IgG group (Figure 4A–F). Total Smad2/3 levels remained unchanged between the two groups (Figure 4A,C). Moreover, α-SMA and collagen I staining demonstrated that Mab2F1 treatment significantly reduced the laser-induced fibrosis areas relative to the IgG group (Figure 4G–I). These results indicated that blockade of canonical Wnt signaling inhibited the laser-induced subretinal fibrosis.

3.5 | Overexpression of sVLDLR in the IPM attenuated laser-induced subretinal fibrosis

To investigate if overexpressed sVLDLR decreases subretinal fibrosis, a transgenic mouse model (*sVLDLR-Tg*) overexpressing human *VLDLR* ectodomain in the photoreceptors was generated. The transgene vector was shown in Figure

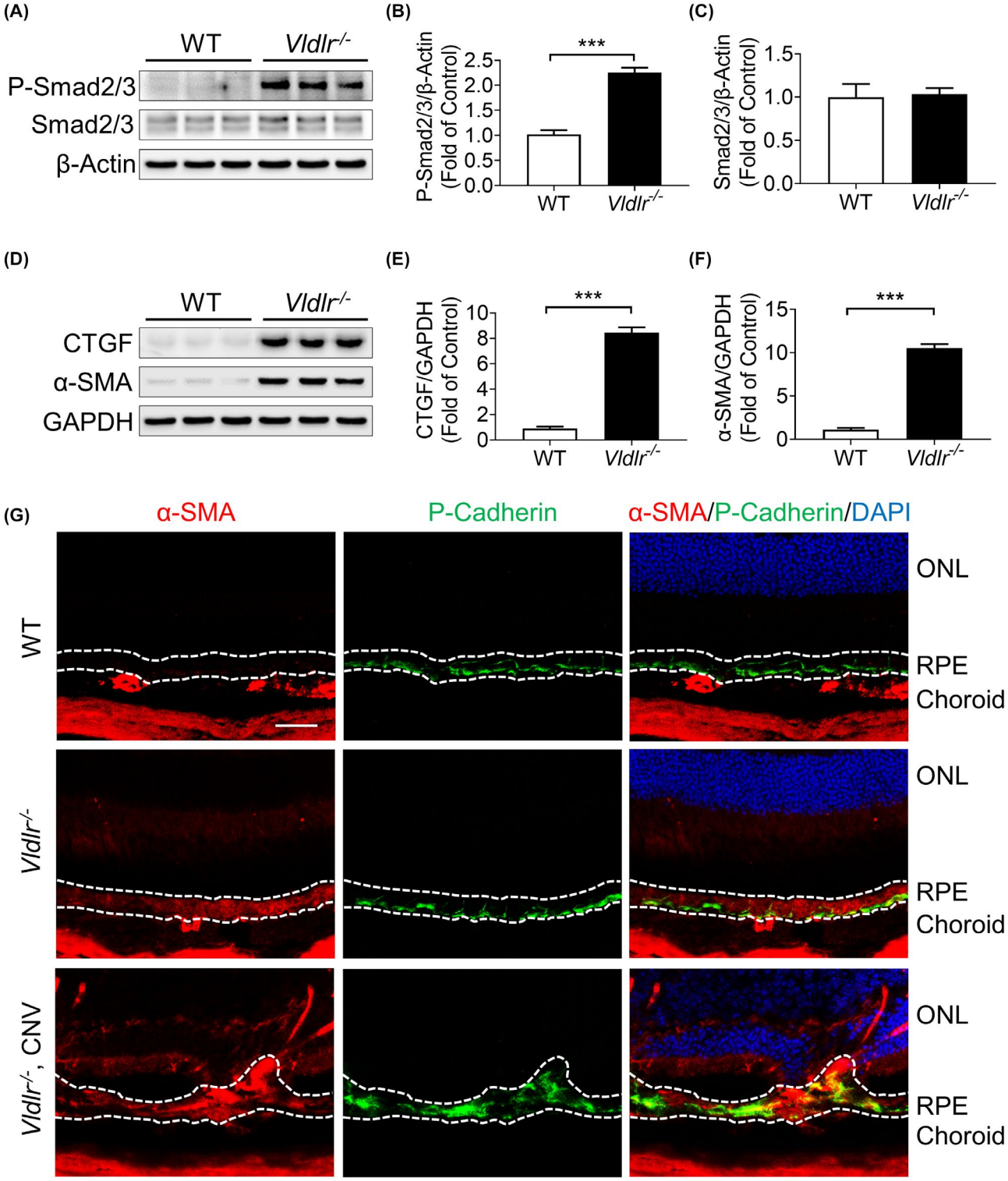

FIGURE 1 Overactivated TGF-β/Smad signaling and fibrosis in the subretinal region of *Vldlr*$^{-/-}$ mice. (A) Representative images of Western blotting for P-Smad2/3 and total Smad2/3 in the RPE sheets of 3-month-old *Vldlr*$^{-/-}$ mice and WT littermates are shown. (B, C) Protein levels of P-Smad2/3 and total Smad2/3 in (A) were quantified by densitometry and normalized to β-Actin levels ($n = 6$). Both bands of total Smad2/3 were used for quantification. (D–F) Protein levels of CTGF and α-SMA in isolated RPE sheets from 3-month-old *Vldlr*$^{-/-}$ mice and WT littermates were measured by Western blot analysis and quantified by densitometry ($n = 6$). (G) Representative images of immunostaining for α-SMA and P-cadherin in the subretinal areas of 3-month-old *Vldlr*$^{-/-}$ mice (with and without the intrusion of CNV from the choroid into retinas) and WT littermates. P-cadherin is the most abundant cadherin in the RPE layer,[36] and thus, it was used as a marker of RPE cells. The white dashed lines defined the borders of the RPE layer. CNV, choroidal neovascularization; ONL, outer nuclear layer; RPE, retinal pigment epithelium. Scale bar: 50 μm. Data were presented as mean ± SEM. ***$p < .001$

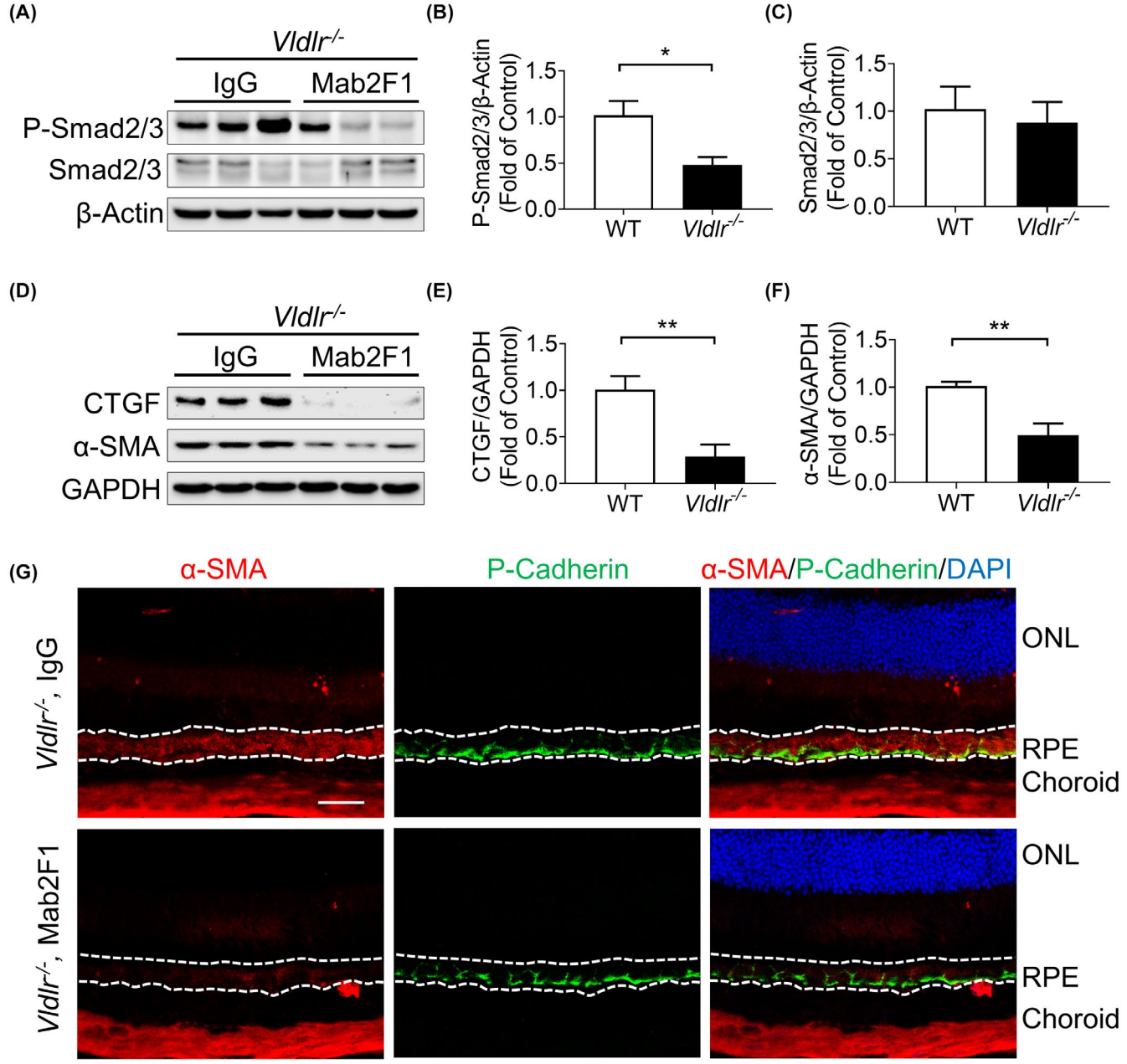

FIGURE 2 Mab2F1 inhibited the profibrotic changes in the subretinal region of $Vldlr^{-/-}$ mice. At day 7 post-intravitreal injection of Mab2F1 (6 μg/eye) or nonspecific mouse IgG into 3-month-old $Vldlr^{-/-}$ mice, the RPE sheets and eyecups were isolated for Western blot analysis and immunohistochemistry, respectively. (A) Representative images of Western blotting for P-Smad2/3 and total Smad2/3 in the RPE tissues of $Vldlr^{-/-}$ mice treated with normal mouse IgG or Mab2F1. (B, C) Protein levels of P-Smad2/3 and both bands of total Smad2/3 in (A) were quantified by densitometry and normalized to β-Actin levels ($n = 6$). (D–F) Similarly, protein levels of CTGF and α-SMA in isolated RPE sheets of $Vldlr^{-/-}$ mice treated with Mab2F1 or mouse IgG were measured by Western blot analysis and quantified by densitometry ($n = 6$). (G) Representative images of immunostaining for α-SMA and P-cadherin in the subretinal areas of $Vldlr^{-/-}$ mice treated with Mab2F1 or mouse IgG were shown. The white dashed lines defined the borders of the RPE layer. ONL, outer nuclear layer; RPE, retinal pigment epithelium. Scale bar: 50 μm. Data were presented as mean ± SEM. $^{*}p < .05$, $^{**}p < .01$

S1A. The positive genotyping results of the two founders were shown in Figure S1B. There was an increased sVLDLR level in the IPM of *sVLDLR-Tg* mice compared to WT littermates (Figure 5A–C). Protein levels of nonphosphorylated-β-catenin were decreased in the RPE-choroid complexes of *sVLDLR-Tg* mice relative to those in WT littermates (Figure S1C,D). Seven days after laser induction, protein levels of P-Smad2/3, CTGF, and α-SMA were significantly decreased in the *sVLDLR-Tg* mice relative to those in WT littermates (Figure 5D–I). Total Smad2/3 levels remained unchanged between genotypes (Figure 5D,F). *sVLDLR-Tg* mice showed a significant reduction of laser-induced

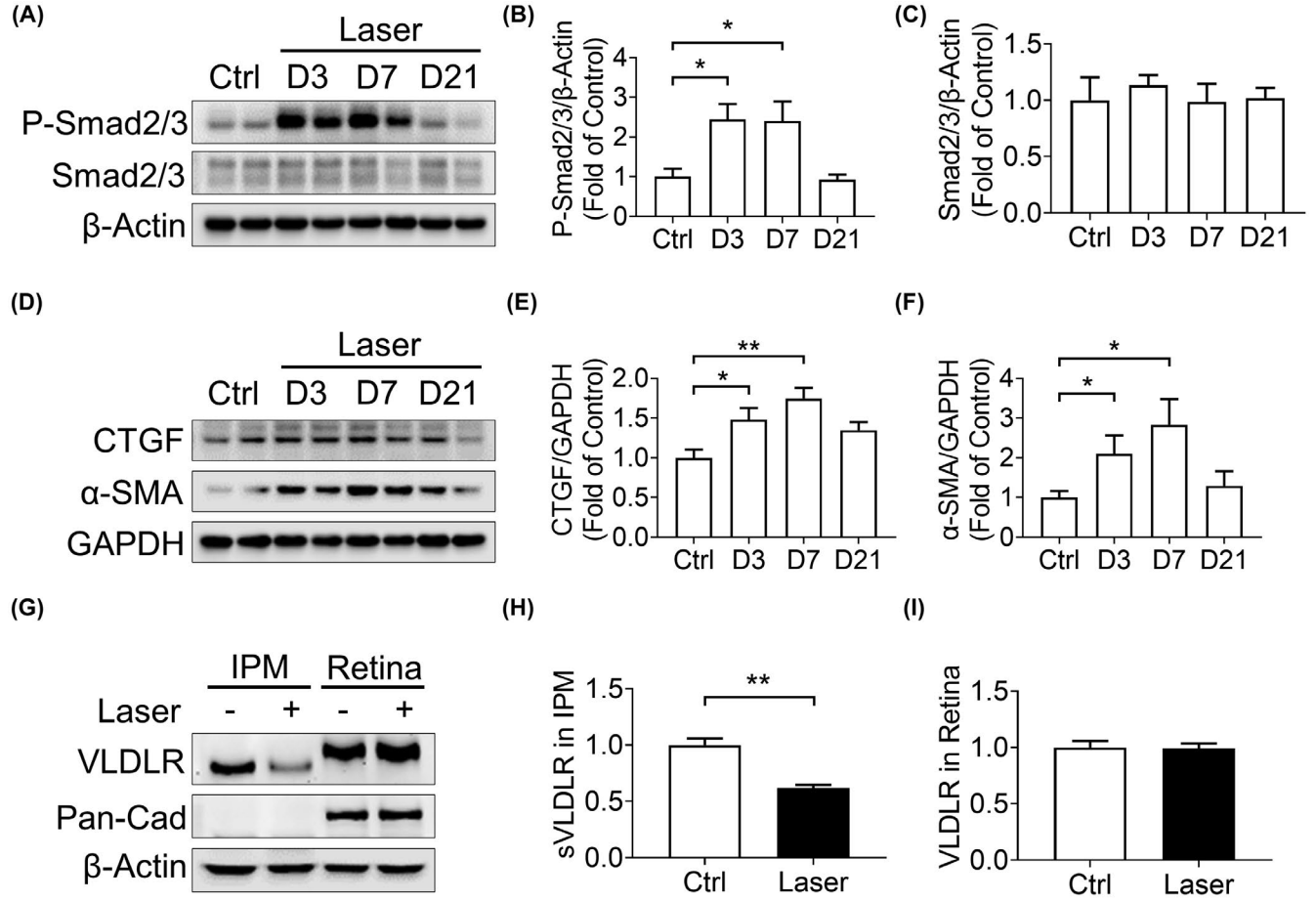

FIGURE 3 Reduced sVLDLR levels in the IPM and subretinal fibrosis in the laser-induced CNV model. Three-month-old WT C57BL/6J mice were subjected to laser induction. At indicated days, the RPE of laser-induced mice or sham-operated littermates (Ctrl) were harvested for Western blot analysis. (A) Representative images of Western blotting for P-Smad2/3 and total Smad2/3 in the RPE of mice 3, 7, and 21 days post-laser induction. (B, C) Protein levels of P-Smad2/3 and total Smad2/3 in (A) were quantified by densitometry and normalized to β-Actin levels ($n = 6$). Both bands of total Smad2/3 were used for quantification. (D–F) Protein levels of CTGF and α-SMA in the RPE tissues were measured by Western blot analysis and quantified by densitometry ($n = 6$). (G) Representative images of Western blotting for sVLDLR in the IPM and the full-length VLDLR in the retinas of laser-induced CNV and sham-operated mice were shown. Samples were harvested at 7 days post-laser induction. Pan-cadherin (Pan-Cad) was used as a plasma membrane marker. (H, I) Protein levels of sVLDLR and the full-length VLDLR in (G) were quantified by densitometry ($n = 3$). Data were presented as mean ± SEM. $^*p < .05$, $^{**}p < .01$

vascular leakage as measured by fluorescein angiography (Figure 5J,K). Furthermore, overexpressed sVLDLR decreased the fibrosis area as measured by α-SMA and collagen I staining in the flat-mounted eyecup at day 7 post-laser induction (Figure 5L–N) as well as at day 21 post-laser induction (Figure S1F–H). These results indicated that sVLDLR overexpression in the IPM attenuated the subretinal fibrosis in the laser-induced CNV model.

3.6 | Wnt ligand promoted TGF-β2-induced fibrosis markers in human RPE cells

Compared to the vehicle group, TGF-β2-treated ARPE-19 cells showed significantly increased levels of P-Smad2/3, and downstream profibrotic genes, including CTGF and α-SMA (Figure 6). The Wnt3A conditioned medium (WCM) was used to activate Wnt signaling. WCM treatment promoted TGF-β2-induced increase of P-Smad2/3, CTGF, and α-SMA levels (Figure 6). Total Smad2/3 levels were non-significantly different between groups (Figure 6A,C). These results suggested that Wnt and TGF-β signaling conferred the cooperative effect in inducing fibrosis in RPE cells.

3.7 | Mab2F1 suppressed the profibrotic effect of Wnt signaling in human RPE cells

CTGF levels were elevated in WCM-treated ARPE19 cells relative to the LCM control (Figure 7A,B).

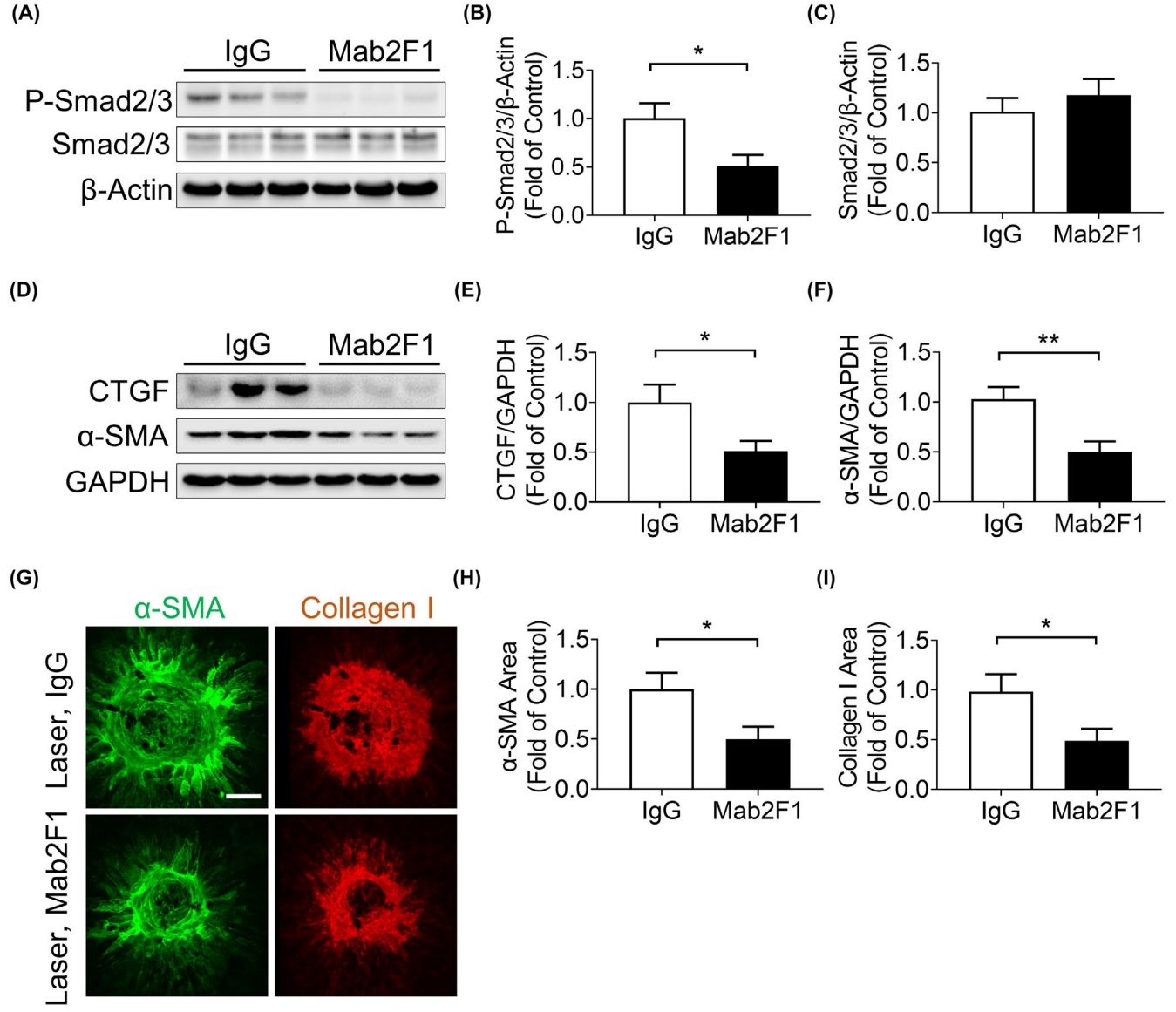

FIGURE 4 Mab2F1 alleviated subretinal fibrosis in the laser-induced CNV model. Two days after laser induction, Mab2F1 (6 μg/eye) or nonspecific mouse IgG was injected into the vitreous of WT C57BL/6J mice. On day 7 post-laser induction, the RPE tissues were harvested for Western blot analysis. (A) Representative images of Western blotting for P-Smad2/3 and total Smad2/3 in the RPE tissues of the laser-induced CNV model treated with Mab2F1 or mouse IgG as the control. (B, C) Protein levels of P-Smad2/3 and total Smad2/3 in (A) were quantified by densitometry and normalized to β-Actin levels ($n = 6$). Both bands of total Smad2/3 were used for quantification. (D–F) Protein levels of CTGF and α-SMA in the RPE tissues were measured by Western blot analysis and quantified by densitometry ($n = 6$). (G) Representative immunostaining for α-SMA and collagen I in the flat-mounted eyecup from the laser-induced CNV model treated with the mouse IgG or Mab2F1. (H, I) The relative areas of α-SMA and collagen I staining in (G) were quantified by ImageJ software ($n = 6$). Scale bar: 50 μm. Data were presented as mean ± SEM. *$p < .05$, **$p < .01$

Mab2F1 treatment inhibited the WCM-induced increase of CTGF (Figure 7A,B). Mab2F1 treatment also attenuated the synergistic effect between WCM and TGF-β2 in inducing P-Smad2/3, CTGF, and α-SMA in ARPE-19 cells (Figure 7C–H). These results indicated that inhibition of Wnt signaling suppressed TGF-β-induced upregulation of profibrotic markers in RPE cells.

3.8 | *LRP6* KO reduced Wnt ligand- and TGF-β2-induced fibrosis markers in human RPE cells

To investigate if LRP6 is required for TGF-β2-mediated fibrosis, an ARPE-19 cell line with *LRP6* KO was generated using the CRISPR/Cas9 technology.[18] *LRP6* KO significantly blocked WCM-induced TCF/β-catenin activity (Figure S3).

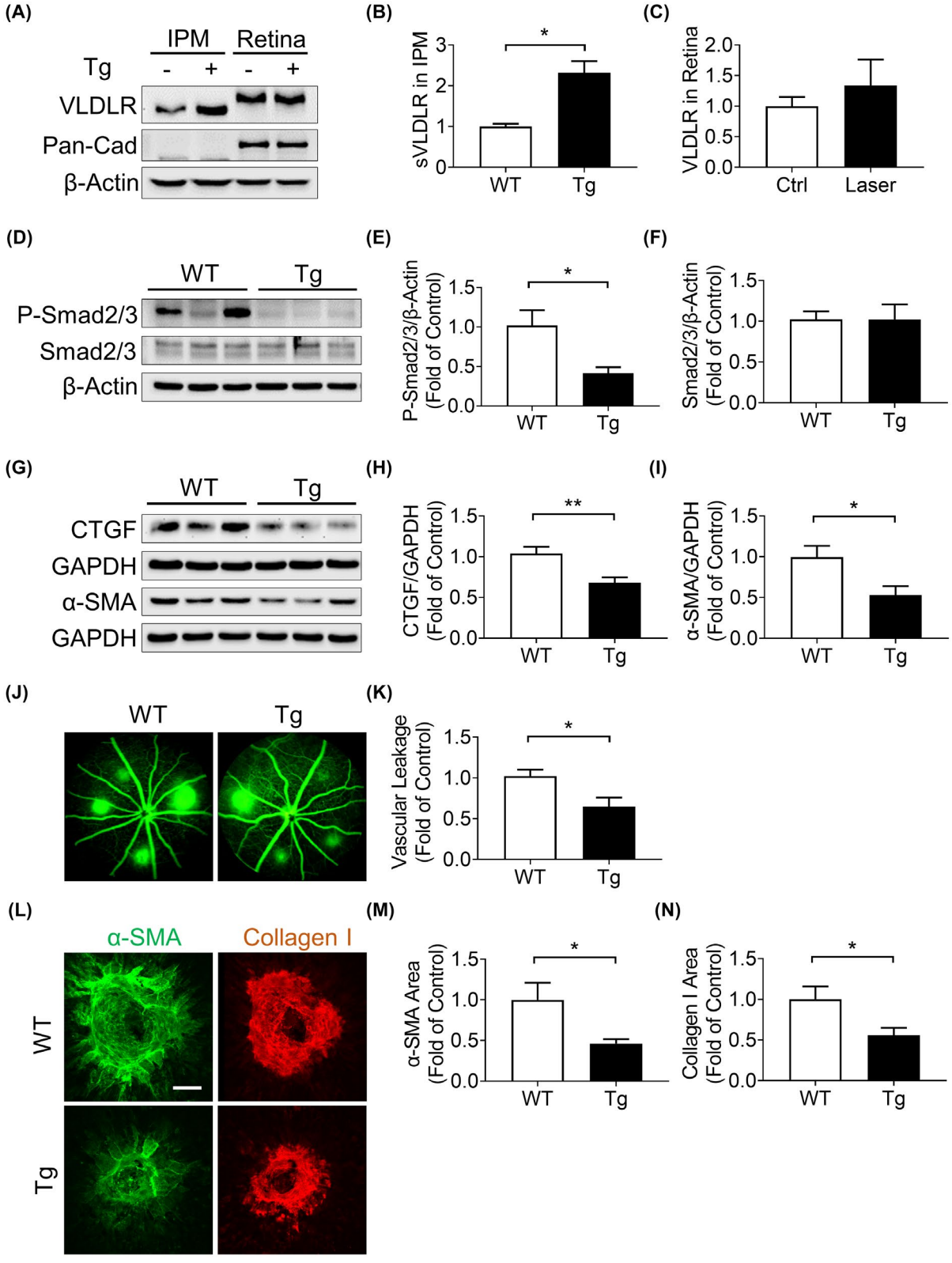

Protein levels of CTGF and α-SMA were significantly decreased in *LRP6* KO ARPE-19 cells compared to WT ARPE-19 cells (Figure 8A–C). In WCM-treated cells, *LRP6* KO suppressed the WCM-induced CTGF level (Figure 8A,B). In TGF-β2-treated cells, *LRP6* KO diminished TGF-β2-induced P-Smad2/3, CTGF, and α-SMA levels (Figure 8D–I). The total Smad2/3 levels remained non-significantly different among the groups (Figure 8D,F). Moreover, *LRP6* KO abolished the synergistic effect between WCM and TGF-β2 in increasing CTGF and α-SMA levels in ARPE-19 cells (Figure 8J–L). These results suggested that LRP6-dependent Wnt signaling was essential for TGF-β-mediated fibrosis.

FIGURE 5 Overexpression of sVLDLR in the IPM attenuated laser-induced subretinal fibrosis. Three-week-old *sVLDLR-Tg* mice and WT littermates were administered water containing 2 mg/ml doxycycline for 2 weeks to induce sVLDLR overexpression. Then, laser induction was performed. Seven days after laser induction, the RPE tissues were harvested for Western blot analysis and immunohistochemistry. (A) Representative images of Western blotting for sVLDLR in the IPM and the full-length VLDLR in the retinas of *sVLDLR-Tg* mice and WT littermates. Pan-cadherin (Pan-Cad) was used as a plasma membrane marker. (B, C) Protein levels of sVLDLR in the IPM and the full-length VLDLR in retinas in (A) were quantified by densitometry ($n = 3$). (D) Representative images of Western blotting for P-Smad2/3 and total Smad2/3 in the RPE tissues of laser-treated *sVLDLR-Tg* mice and WT littermates. (E, F) Protein levels of P-Smad2/3 and total Smad2/3 were quantified by densitometry and normalized to β-Actin ($n = 6$). Both bands of total Smad2/3 were used for quantification. (G–I) Similarly, protein levels of CTGF and α-SMA in the RPE-choroid complexes were measured by Western blot analysis and quantified by densitometry ($n = 6$). (J) Representative images of fluorescein angiography in laser-treated *sVLDLR-Tg* mice and WT littermates are shown. (K) Relative areas of fluorescein leakage in (J) were quantified by ImageJ software ($n = 6$). (L) Representative immunostaining for α-SMA and collagen I of the flat-mounted eyecup from the laser-induced WT and *sVLDLR-Tg* mice are shown. (M, N) The relative areas of α-SMA and collagen I staining were quantified by ImageJ ($n = 6$). Tg, transgenic mice; WT, wild-type littermates. Scale bar: 50 μm. Data were presented as mean ± SEM. $^{*}p < .05$, $^{**}p < .01$

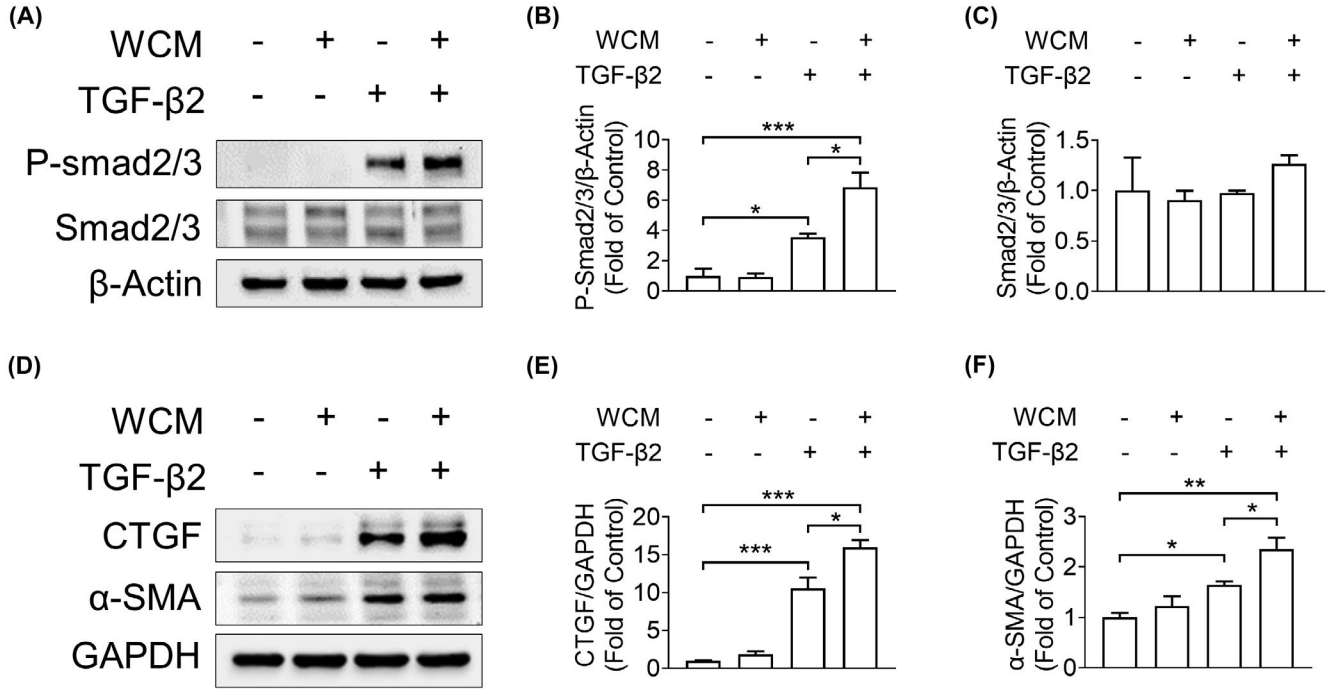

FIGURE 6 WCM promoted TGF-β2-induced fibrosis markers in human RPE cells. ARPE-19 cells were treated with 40% WCM or LCM in the presence of 1 ng/ml TGF-β2 or vehicle as the control for 24 h. (A) Representative images of Western blotting for P-Smad2/3 and total Smad2/3 in ARPE-19 cells were shown. (B, C) Protein levels of P-Smad2/3 and total Smad2/3 in (A) were quantified by densitometry and normalized to β-Actin levels ($n = 3$). Both bands of total Smad2/3 were used for quantification. (D–F) Protein levels of CTGF and α-SMA were measured in ARPE-19 cells by Western blot analysis and quantified by densitometry ($n = 3$). Data were presented as mean ± SEM. $^{*}p < .05$, $^{**}p < .01$, $^{***}p < .001$

3.9 | Disruption of *VLDLR* gene expression promoted TGF-β2-induced fibrosis markers in RPE cells

To determine the direct effect of VLDLR on the expression of fibrotic factors in RPE cells, primary RPE cells from *Vldlr*$^{-/-}$ mice and WT littermates were used. Primary RPE cells from *Vldlr*$^{-/-}$ mice showed more prominent TGF-β2-induced increases of P-Smad2/3, CTGF, and α-SMA levels relative to primary RPE cells from WT littermates (Figure 9A–F). These results indicated that disruptive VLDLR expression promoted TGF-β signaling-mediated fibrosis in RPE cells.

3.10 | sVLDLR overexpression suppressed the synergistic effect of Wnt/β-catenin and TGF-β2 signaling in promoting fibrosis in human RPE cells

To evaluate the antifibrotic effect of sVLDLR, ARPE-19 cells were infected with adenovirus expressing sVLDLR

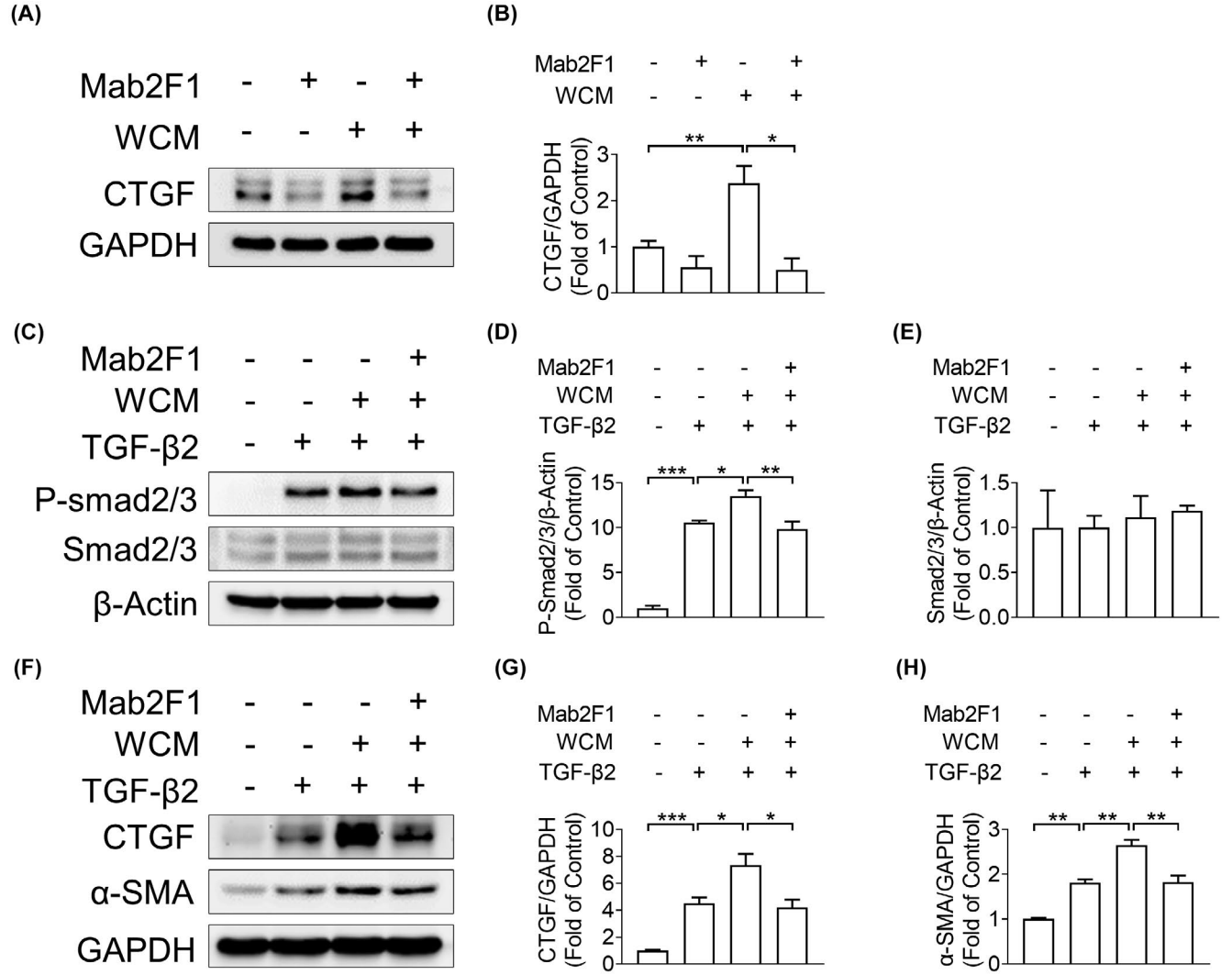

FIGURE 7 Mab2F1 suppressed the profibrotic effect of Wnt signaling in human RPE cells. (A, B) ARPE-19 cells were treated with 40% WCM or LCM in the presence of 50 μg/ml Mab2F1 or nonspecific mouse IgG as the control for 24 h. Protein levels of CTGF were measured by Western blot analysis and quantified by densitometry ($n = 3$). (C–E) ARPE-19 cells were pre-treated with 40% WCM or LCM in the presence of 50 μg/ml Mab2F1 or nonspecific mouse IgG as the control for 24 h. Then, ARPE-19 cells were treated with 1 ng/ml TGF-β2 or vehicle as control for 1 h. (D, E). Protein levels of P-Smad2/3 and total Smad2/3 were measured by Western blot analysis and quantified by densitometry ($n = 3$). Both bands of total Smad2/3 were used for quantification. (F–H) ARPE-19 cells were treated with 1 ng/ml TGF-β2 or vehicle as control, with or without 40% WCM and 50 μg/ml Mab2F1 for 24 h. Protein levels of CTGF and α-SMA were measured by Western blot analysis and quantified by densitometry ($n = 3$). Data were presented as mean ± SEM. *$p < .05$, **$p < .01$, ***$p < .001$

or adenovirus expressing RFP as control. As shown in Figure 10A–C, overexpression of sVLDLR reduced basal levels of CTGF and α-SMA in ARPE-19 cells. Moreover, increased sVLDLR suppressed WCM-upregulated CTGF levels (Figure 10A,B). Furthermore, overexpression of sVLDLR reduced P-Smad2/3, CTGF, and α-SMA in ARPE-19 cells treated with WCM and TGF-β2 (Figure 10D–I). Notably, the protein level of total Smad2/3 was significantly decreased in ARPE-19 cells with sVLDLR overexpression relative to RFP overexpression (Figure 10D,F). These results indicated that overexpression of sVLDLR suppressed the synergistic effect between the Wnt/β-catenin and TGF-β signaling pathways.

4 | DISCUSSION

For the first time, this study demonstrated that the over-activated TGF-β/Smad pathway and fibrosis were present in the sub-retina of *Vldlr*$^{-/-}$ mice (Figure 1). In primary RPE cells, disruption of VLDLR expression increased TGF-β/Smad-mediated profibrotic markers, indicating that VLDLR conferred an antifibrotic effect in the RPE (Figure 9). Furthermore, the present study was the first to demonstrate the reduced sVLDLR level in the IPM of the laser-induced CNV model (Figure 3). Overexpressed sVLDLR in the IPM of our newly generated *sVLDLR-Tg* mice prevented laser-induced subretinal fibrosis, suggesting

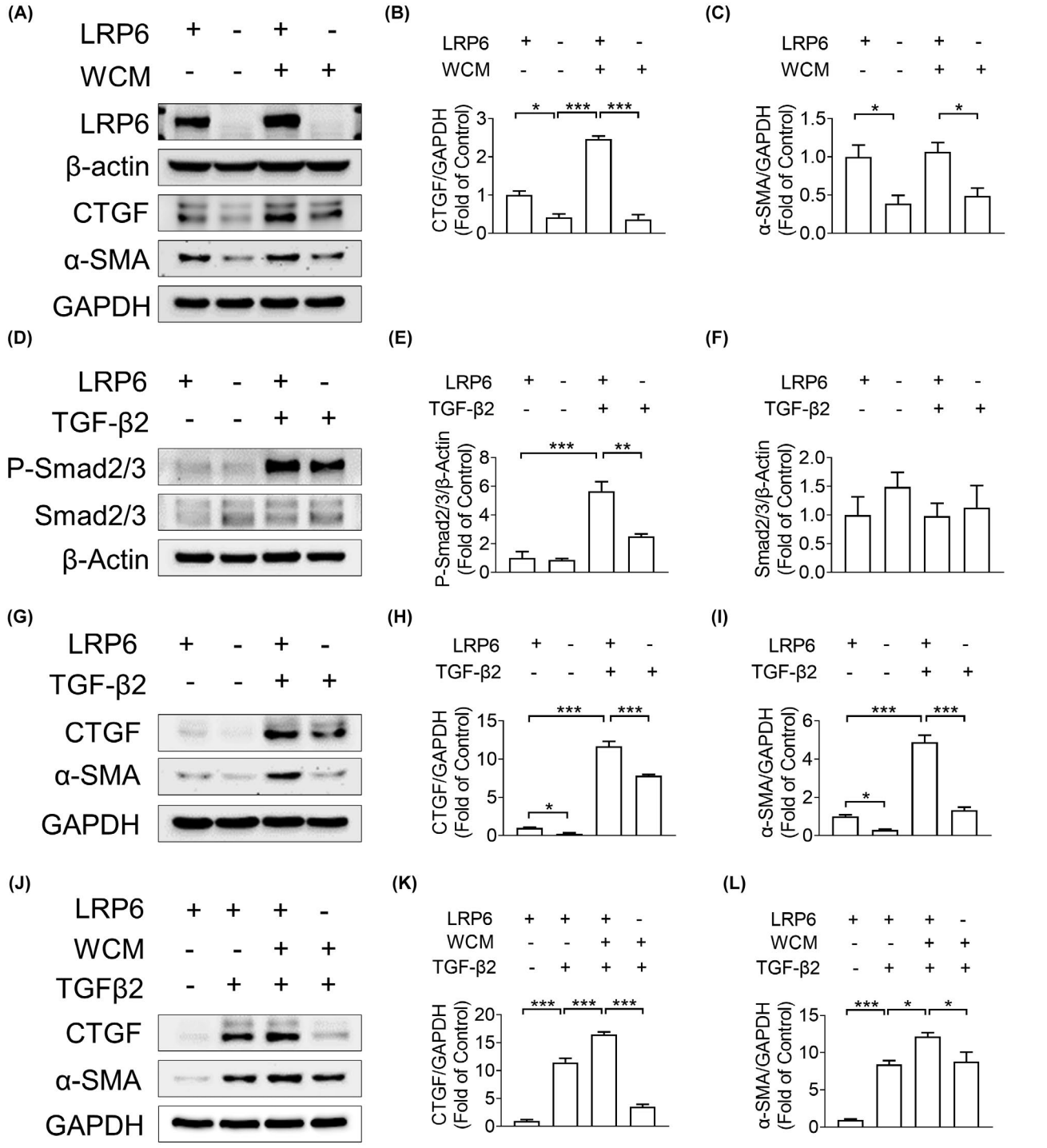

FIGURE 8 *LRP6* KO decreased WCM and TGF-β2-induced fibrosis factors in human RPE cells. WT ARPE-19 cells and ARPE-19 cells with *LRP6* KO were used. (A) Representative images of Western blotting for LRP6, CTGF, and α-SMA in the cells treated with 40% WCM or LCM as the control for 24 h. (B, C) Protein levels of CTGF and α-SMA in (A) were quantified by densitometry and normalized to β-Actin levels ($n = 3$). (D) Representative images of Western blotting for P-Smad2/3 and total Smad2/3 in the WT and *LRP6* KO ARPE-19 cells in the presence of 1 ng/ml TGF-β2 or vehicle as the control for 1 h. (E, F) Protein levels of P-Smad2/3 and total Smad2/3 in (D) were quantified by densitometry ($n = 3$). Both bands of total Smad2/3 were used for quantification. (G) Representative images of Western blotting for CTGF and α-SMA in the WT and *LRP6* KO ARPE-19 cells treated with 1 ng/ml TGF-β2 or vehicle as the control for 24 h. (H, I) Protein levels of CTGF and α-SMA in (G) were quantified by densitometry ($n = 3$). (J–L) WT and *LRP6* KO ARPE-19 cells were treated with 1 ng/ml TGF-β2 or vehicle in the presence of 40% WCM or LCM as the control for 24 h. (J) Representative images of Western blotting for CTGF and α-SMA in the treated cells were shown. (K, L) Protein levels of CTGF and α-SMA in (J) were quantified by densitometry ($n = 3$). Data were presented as mean ± SEM. *$p < .05$, **$p < .01$, ***$p < .001$

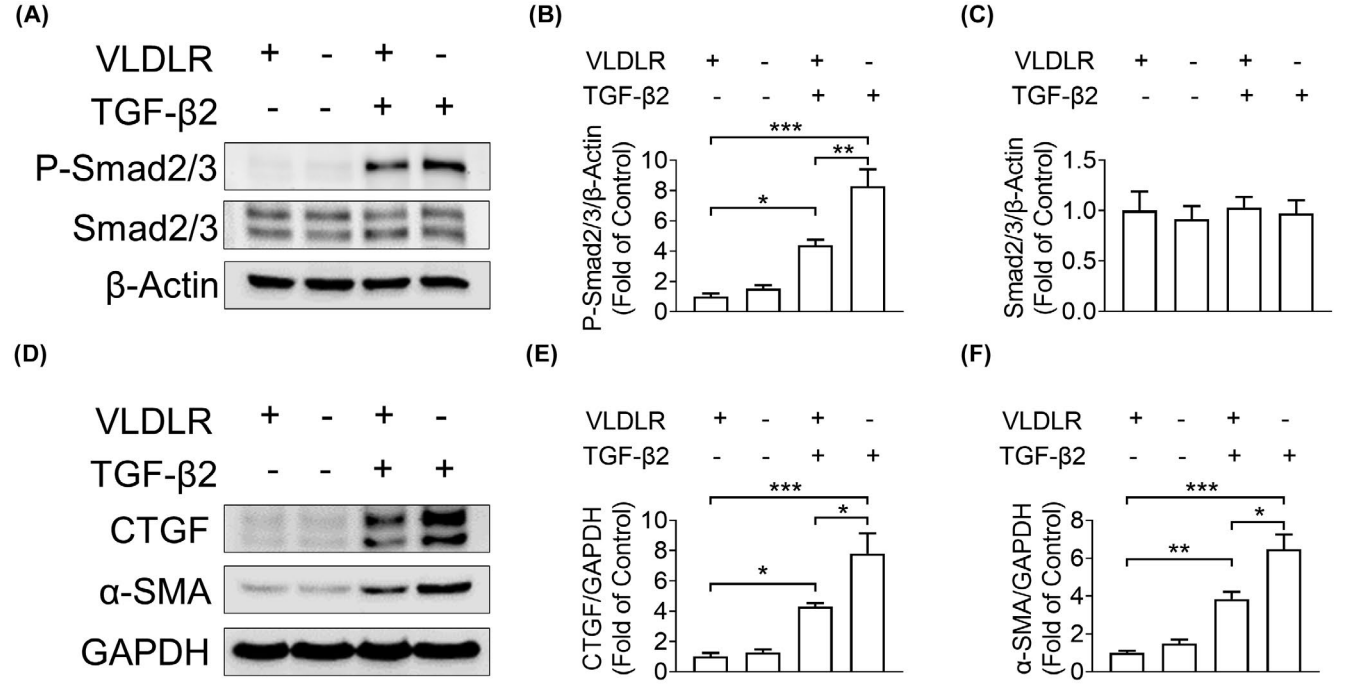

FIGURE 9 Disruption of *VLDLR* gene expression promoted TGF-β2-induced fibrosis factors in RPE cells. The primary RPE cells were harvested from 4- to 6-week-old $Vldlr^{-/-}$ mice and WT littermates and cultured for 10 days to reach the confluence. (A) Representative images of Western blotting for P-Smad2/3 and total Smad2/3 in mouse primary RPE cells treated with 1 ng/ml TGF-β2 or vehicle as the control for 1 h. (B, C) Protein levels of P-Smad2/3 and total Smad2/3 in (A) were quantified by densitometry and normalized to β-Actin levels ($n = 3$). Both bands of total Smad2/3 were used for quantification. (D–F) Mouse primary RPE cells treated with 1 ng/ml TGF-β2 or vehicle as the control for 24 h. Protein levels of CTGF and α-SMA were measured in mouse primary RPE cells by Western blot analysis and quantified by densitometry ($n = 3$). Data were presented as mean ± SEM. *$p < .05$, **$p < .01$, ***$p < .001$

that sVLDLR shed into the IPM was responsible for the antifibrotic effect (Figure 5). Concerning molecular mechanism, we found that the antifibrotic effect of sVLDLR was, at least in part, through the inhibition of canonical Wnt signaling. Blockade of Wnt signaling by an anti-LRP6 antibody suppressed subretinal fibrosis in $Vldlr^{-/-}$ mice and the laser-induced CNV model (Figures 2 and 4). Consistent with these findings, activation of Wnt signaling promoted, whereas inhibition of Wnt signaling by the disruption of LRP6 suppressed TGF-β/Smad-mediated fibrosis in RPE cells (Figures 6–8). These results led us to propose that reduced sVLDLR level contributed to the overactivated canonical Wnt signaling, which promoted the TGF-β/Smad-mediated fibrosis in subretinal regions in nAMD (Figure 11).

VLDLR plays a crucial role in many pathophysiological processes, including lipid metabolism, neuronal migration, and cardiac hypertrophy.[42–44] Several groups have reported that mice with *Vldlr* gene deficiency manifested human nAMD-like phenotypes, such as subretinal NV, retinal inflammation, and degeneration.[20,45,46] The current study was the first to show that by the age of 3 months, $Vldlr^{-/-}$ mice developed the subretinal fibrosis accompanied by aberrant activation of the TGF-β/Smad pathway (Figure 1). Our results suggested that $Vldlr^{-/-}$ mice could serve as a subretinal fibrotic model for investigating antifibrotic therapies. The enhanced α-SMA immunostaining signals were detected in both the RPE layer and NV region of $Vldlr^{-/-}$ mice, indicating that *Vldlr* KO may induce RPE acquisition of α-SMA-positive myofibroblast-like phenotypes and fibrovascularization (Figure 1). Consistent with in vivo results, we found that TGF-β-induced fibrosis markers were enhanced by *Vldlr* KO in primary mouse RPE cells (Figure 9). Overall, these findings indicated that deficiency of VLDLR expression promoted subretinal fibrosis.

In a previous study, we reported that human and mouse retinas express exclusively the VLDLR isoform II.[25] Compared to the full-length VLDLR isoform I, the VLDLR isoform II lacks the O-linked glycosylated domain at the juxtamembrane part, resulting in a higher shedding of VLDLR ectodomain (sVLDLR) into the extracellular space.[25] Our study indicated that sVLDLR might have a context-specific physiological function in the retina. A prior study showed that VLDLR was abundant in the outer segment layer and outer nuclear layer near the IPM region relative to other retinal layers.[45] Our previous work also showed that sVLDLR was naturally present in the IPM of bovine and murine eyes.[25] As demonstrated by other researchers and us, laser-induced CNV developed Wnt

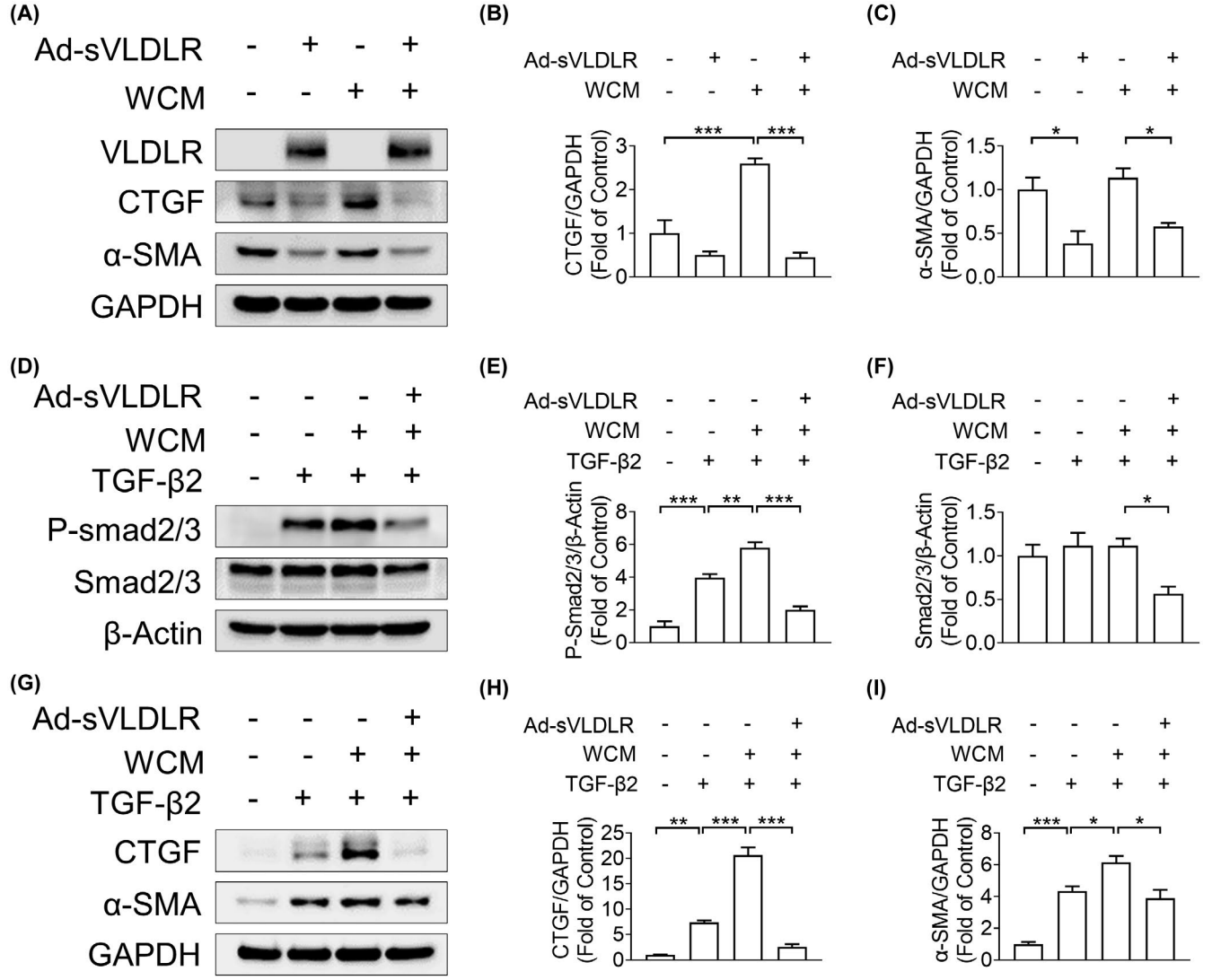

FIGURE 10 sVLDLR suppressed the synergistic profibrotic effect of Wnt and TGF-β signaling in human RPE cells. (A–C) ARPE-19 cells were infected with adenovirus overexpressing sVLDLR (Ad-sVLDLR) or adenovirus overexpressing RFP (Ad-RFP) with the MOI of 50 for 48 h. Then, the cells were treated with 40% WCM or LCM as the control for 24 h. (A) Representative images of Western blotting for VLDLR, CTGF, and α-SMA in the treated ARPE-19 cells are shown. (B, C) Protein levels of CTGF and α-SMA in (A) were quantified by densitometry and normalized to GAPDH ($n = 3$). (D–I) ARPE-19 cells were infected with Ad-sVLDLR or Ad-RFP for 48 h. (D) Then, the cells were treated with 40% WCM or LCM in the presence of 1 ng/ml TGF-β2 or vehicle as the control for 1 h. Representative images of Western blotting for P-Smad2/3 and total Smad2/3 in treated ARPE-19 cells were shown. (E, F) Protein levels of P-Smad2/3 and total Smad2/3 in (D) were quantified by densitometry and normalized to β-Actin levels ($n = 3$). Both bands of total Smad2/3 were used for quantification. (G) After adenovirus infection, cells were treated with 40% WCM or LCM in the presence of 1 ng/ml TGF-β2 or vehicle as the control for 24 h. Representative images of Western blotting for CTGF and α-SMA were shown. (H, I) Protein levels of CTGF and α-SMA in (G) were quantified by densitometry and normalized to GAPDH ($n = 3$). Data were presented as mean ± SEM. *$p < .05$, **$p < .01$, ***$p < .001$

signaling-mediated subretinal fibrosis.[16,37] However, the precise molecular mechanism underlying the aberrant activation of Wnt signaling in CNV models remains elusive. In the present study, we proposed that sVLDLR shedding from photoreceptors into the IPM may play an essential role in regulating the local homeostasis. Reduced levels of sVLDLR in the IPM may account for overactivated Wnt signaling and subretinal fibrosis in the laser-induced CNV model. To test our hypothesis, we measured the sVLDLR level in the IPM of the laser-induced CNV model. Notably, we found that the sVLDLR level in the IPM was markedly decreased in the laser-induced CNV model. We also applied an sVLDLR overexpression system to prove our hypothesis. By re-analyzing a single-cell RNA sequencing database of murine retinal samples,[47] we identified that rod photoreceptor cells have the highest level of

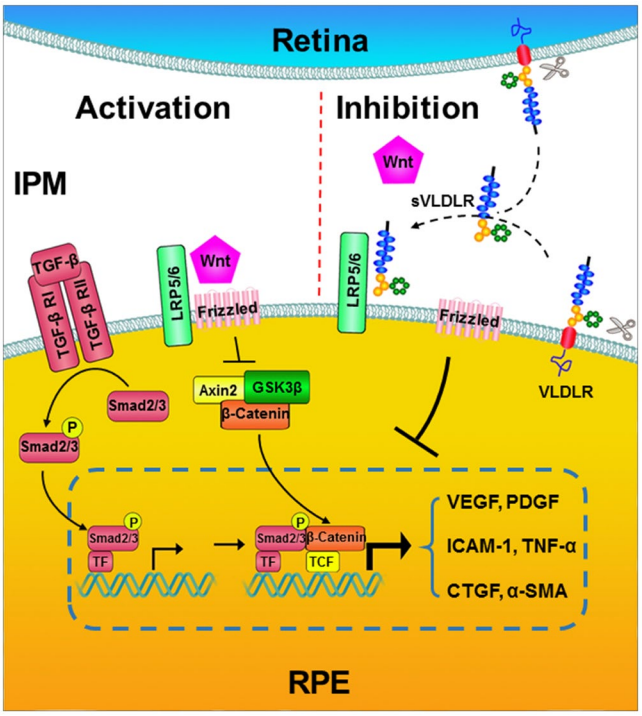

FIGURE 11 Schematics showing that VLDLR inhibits Wnt signaling-enhanced subretinal fibrosis. The Wnt signaling is activated by binding of Wnt ligands to the frizzled and LRP5/6 co-receptors. It stabilizes the cytoplasmic β-catenin and increases the β-catenin translocation into the nucleus, resulting in the activation of Wnt target genes, including pro-inflammatory factors, pro-angiogenic factors, and profibrotic factors.[28,39,40] Wnt activation also stabilizes phosphorylation of Smad2/3. Wnt and TGF-β signaling play a synergistic effect in inducing profibrotic markers. VLDLR sheds its soluble extracellular domain, soluble VLDLR (sVLDLR), to function as an endogenous inhibitor of canonical Wnt signaling by binding with a Wnt co-receptor, LRP6.[24] In nAMD models, there are overactivated Wnt signaling and fibrosis in the subretinal space.[16,17,41] However, the regulation of Wnt signaling and fibrosis in the sub-retinas of nAMD models remains incompletely understood. This study shows that sVLDLR shedding into the IPM is decreased in the laser-induced CNV, contributing to Wnt signaling overactivation and fibrosis. CTGF, connective tissue growth factor; ICAM-1, intercellular adhesion molecule 1; IPM, interphotoreceptor matrix; LRP, low-density lipoprotein receptor-related protein; PDGF, platelet-derived growth factor; sVLDLR, soluble very low-density lipoprotein receptor; TCF, T-cell factor; TF, transcription factor; TGF-βR, transforming growth factor-beta receptor; TNF-α, Tumor necrosis factor-alpha; VEGF, vascular endothelial growth factor; α-SMA, alpha-smooth muscle actin

endogenous VLDLR expression. Therefore, we designed a rhodopsin promoter-driven sVLDLR overexpression system in transgenic mice (Figure S1). We found that overexpressed sVLDLR in the retinas contributed to higher sVLDLR levels in the IPM, suppressing the overactivated Wnt signaling and subretinal fibrosis in the laser-induced CNV model (Figures 5 and S1). In concert with in vivo findings, sVLDLR overexpression ameliorated Wnt3A-induced upregulation of profibrotic markers in ARPE-19 cells (Figure 10). sVLDLR confers an antifibrotic effect in the laser-induced CNV model, at least in part, through inhibition of Wnt signaling.

Canonical Wnt signaling promotes fibrosis and scarring formation in various tissues and organs, such as cardiac, renal, and pulmonary fibrosis.[11,48] In this study, we demonstrated that Wnt signaling is required for subretinal fibrosis. Wnt signaling comprises 19 Wnt ligands, 10 frizzled receptors, and 2 co-receptors.[28] We manipulated Wnt signaling by blocking Wnt co-receptor, LRP6, since (1) activation of canonical Wnt signaling required either LRP5 or LRP6[28]; (2) sVLDLR was reported to confer an inhibitory effect on Wnt signaling by heterodimerizing with LRP6[24]; (3) The LRP6-blocking antibody, Mab2F1, was sufficient to alleviate Wnt signaling-mediated NV and inflammation in the laser-induced CNV model, and vascular leakage and inflammation in streptozotocin-induced diabetic retinopathy.[16,28] This study demonstrated that Mab2F1 inhibited subretinal fibrosis in *Vldlr*$^{-/-}$ mice and mice with laser-induced CNV (Figures 2 and 4). In vitro, Mab2F1 inhibited the Wnt3A-induced increase of CTGF in ARPE-19 cells (Figure 7). To confirm our findings with Mab2F1, ARPE-19 cells with *LRP6* KO by the CRISPR/Cas9 technology were generated.[18] *LRP6* KO ARPE-19 cells showed lower basal levels of CTGF and α-SMA relative to WT ARPE-19 cells (Figure 8). Moreover, *LRP6* KO also inhibited Wnt3A-induced upregulation of CTGF (Figure 8). These results indicated that LRP6-dependent canonical Wnt signaling was required for subretinal fibrosis.

sVLDLR represents a strategy of an endogenous peptide, whereas Mab2F1 represents a strategy of monoclonal antibody (mAb). Both approaches demonstrated the potent inhibitory effect on Wnt signaling, providing promising alternative methods other than anti-VEGF therapy. These two distinct approaches have their relative advantages in blocking Wnt signaling. sVLDLR is an endogenous protein fragment with 797 amino acids in length. The size of sVLDLR allows it to block a large region of LRP6 when it binds to LRP6. Given that 19 Wnt ligands interact with different regions of LRP6,[49] sVLDLR may have a broad inhibitory spectrum of Wnt ligands. In addition, the endogenous character of sVLDLR raises little concern about immunogenicity. Moreover, the sVLDLR strategy allows diverse therapeutic administrations, such as nanoparticle-embedded sVLDLR plasmids[50] or adeno-associated virus (AAV). On the other hand, Mab2F1 demonstrated high specificity and stability.[28] It is a mAb against the first two-propeller domains (E1E2) of the human LRP6 extracellular domain.[28] Further studies are needed to strengthen the advantages and avoid disadvantages for both strategies. Future efforts are warranted to identify the minimal

fragment in sVLDLR with Wnt inhibitory effect to minimize unwanted effects such as protein instability or the interference with lipid metabolism.

TGF-β/Smad signaling is the master regulator of fibrogenesis.[35] In ocular studies, previous studies identified overexpression of TGF-β, an increase of P-Smad2, and upregulation of downstream genes, such as α-SMA, CTGF, and collagen I, in the laser-induced CNV model.[37,41,51] In accordance with prior studies, we demonstrated that the TGF-β/Smad pathway was activated, and its downstream gene expression was increased in subretinal tissues of two nAMD models, including *Vldlr*$^{-/-}$ mice and mice with laser-induced CNV (Figures 1 and 3). Specifically, we demonstrated that P-Smad2/3, CTGF, and α-SMA were time-dependently increased in the laser-induced CNV model (Figure 3). In concert with in vivo findings, we showed that TGF-β2 increased levels of P-Smad2/3, CTGF, and α-SMA in ARPE-19 cells (Figure 6). These results indicated that TGF-β/Smad signaling plays a crucial role in subretinal fibrosis. However, TGF-β serves as the multifunctional cytokine in ocular tissues, including retinal neural development and maintenance.[52,53] The direct disruption of the TGF-β pathway may result in retinal degeneration and CNV, leading to unwanted side effects.[54] Our study attempted to provide an alternative strategy to treat TGF-β-mediated fibrosis. It has been reported that the TGF-β pathway and the canonical Wnt signaling pathway interact at multiple levels in the pathways.[55] This study presented the first evidence demonstrating that canonical Wnt signaling is required for TGF-β-mediated subretinal fibrosis. Blockade of Wnt signaling suppressed the TGF-β/Smad pathway in the subretinal space of two nAMD models (Figures 2 and 4). Moreover, we showed that WCM treatment promoted, whereas *LRP6* KO suppressed TGF-β-induced P-Smad2/3 and downstream profibrotic markers, including CTGF and α-SMA in ARPE-19 cells (Figures 6 and 8). We also showed that the synergistic effect between Wnt signaling and TGF-β signaling in ARPE-19 cells was blocked by an LRP6-blocking antibody as well as sVLDLR (Figures 7 and 10). Taken together, Wnt signaling promoted TGF-β-induced subretinal fibrosis by increasing the P-Smad2/3 level. These converging signaling cascades into the nucleus induced the expression of profibrotic genes. This synergistic effect between Wnt and TGF-β pathways can be blocked by sVLDLR overexpression.

In conclusion, overactivated canonical Wnt signaling synergizes with the TGF-β/Smad pathway in the subretinal fibrosis. Our results indicate that inhibition of Wnt/β-catenin signaling could effectively alleviate TGF-β signaling in subretinal fibrosis. sVLDLR confers an antifibrotic effect, at least partially, through inhibition of Wnt signaling. Thus, sVLDLR has a potential application for the antifibrotic treatment in nAMD.

ACKNOWLEDGMENTS

This study was supported by National Institutes of Health (NIH) grants (EY019309, EY012231, EY028949, EY032930, EY032931). The authors would like to thank the technical support from the Diabetic Animal Core and Histology and Image Core of diabetic COBRE (GM122744) and the Vision Core supported by NEI P30 (EY021725).

DISCLOSURES

The authors declare to have no conflict of interest.

AUTHOR CONTRIBUTIONS

Xiang Ma performed experiments, acquired and analyzed data, and wrote the manuscript. Yusuke Takahashi, Wenjing Wu, Jianglei Chen, Wentao Liang, and Marcus Dehdarani conducted experiments and acquired data. Yusuke Takahashi generated adenovirus overexpressing sVLDLR and RFP, and ARPE-19 cells with *LRP6* KO. Marcus Dehdarani purified the Mab2F1 protein. Young-Hwa Shin designed the Tet-on/Tet-off vector for transgenic mice. Siribhinya Benyajati and Jian-xing Ma designed the research, analyzed data, wrote and edited the manuscript. Jian-xing Ma is the guarantor of this work and, as such, has the full access to all the data in this study and takes responsibility for the integrity of these data and the accuracy of the data analysis.

REFERENCES

1. Mitchell P, Liew G, Gopinath B, Wong TY. Age-related macular degeneration. *Lancet*. 2018;392:1147-1159.
2. Hwang JC, Del Priore LV, Freund KB, Chang S, Iranmanesh R. Development of subretinal fibrosis after anti-VEGF treatment in neovascular age-related macular degeneration. *Ophthalmic Surg Lasers Imaging*. 2011;42:6-11.
3. Lim LS, Mitchell P, Seddon JM, Holz FG, Wong TY. Age-related macular degeneration. *Lancet*. 2012;379:1728-1738.
4. Ishikawa K, Kannan R, Hinton DR. Molecular mechanisms of subretinal fibrosis in age-related macular degeneration. *Exp Eye Res*. 2016;142:19-25.
5. Ishikawa M, Sawada Y, Yoshitomi T. Structure and function of the interphotoreceptor matrix surrounding retinal photoreceptor cells. *Exp Eye Res*. 2015;133:3-18.
6. Krebs I, Glittenberg C, Ansari-Shahrezaei S, Hagen S, Steiner I, Binder S. Non-responders to treatment with antagonists of vascular endothelial growth factor in age-related macular degeneration. *Br J Ophthalmol*. 2013;97:1443-1446.
7. Daniel E, Toth CA, Grunwald JE, et al. Risk of scar in the comparison of age-related macular degeneration treatments trials. *Ophthalmology*. 2014;121:656-666.
8. Ma B, Hottiger MO. Crosstalk between Wnt/beta-catenin and NF-kappaB signaling pathway during inflammation. *Front Immunol*. 2016;7:378.
9. Dejana E. The role of Wnt signaling in physiological and pathological angiogenesis. *Circ Res*. 2010;107:943-952.
10. Burgy O, Konigshoff M. The Wnt signaling pathways in wound healing and fibrosis. *Matrix Biol*. 2018;68-69:67-80.

11. Akhmetshina A, Palumbo K, Dees C, et al. Activation of canonical Wnt signalling is required for TGF-beta-mediated fibrosis. *Nat Commun*. 2012;3:735.
12. Nusse R, Clevers H. Wnt/beta-catenin signaling, disease, and emerging therapeutic modalities. *Cell*. 2017;169:985-999.
13. Clevers H, Nusse R. Wnt/beta-catenin signaling and disease. *Cell*. 2012;149:1192-1205.
14. MacDonald BT, Tamai K, He X. Wnt/beta-catenin signaling: components, mechanisms, and diseases. *Dev Cell*. 2009;17:9-26.
15. Tuo J, Wang Y, Cheng R, et al. Wnt signaling in age-related macular degeneration: human macular tissue and mouse model. *J Transl Med*. 2015;13:330.
16. Hu Y, Chen Y, Lin M, Lee K, Mott RA, Ma JX. Pathogenic role of the Wnt signaling pathway activation in laser-induced choroidal neovascularization. *Invest Ophthalmol Vis Sci*. 2013;54:141-154.
17. Chen Y, Hu Y, Lu K, Flannery JG, Ma JX. Very low density lipoprotein receptor, a negative regulator of the wnt signaling pathway and choroidal neovascularization. *J Biol Chem*. 2007;282:34420-34428.
18. Singh HD, Ma JX, Takahashi Y. Distinct roles of LRP5 and LRP6 in Wnt signaling regulation in the retina. *Biochem Biophys Res Commun*. 2021;545:8-13.
19. Haines JL, Schnetz-Boutaud N, Schmidt S, et al. Functional candidate genes in age-related macular degeneration: significant association with VEGF, VLDLR, and LRP6. *Invest Ophthalmol Vis Sci*. 2006;47:329-335.
20. Chen Y, Hu Y, Moiseyev G, Zhou KK, Chen D, Ma JX. Photoreceptor degeneration and retinal inflammation induced by very low-density lipoprotein receptor deficiency. *Microvasc Res*. 2009;78:119-127.
21. Takahashi S, Kawarabayasi Y, Nakai T, Sakai J, Yamamoto T. Rabbit very low density lipoprotein receptor: a low density lipoprotein receptor-like protein with distinct ligand specificity. *Proc Natl Acad Sci USA*. 1992;89:9252-9256.
22. Hussain MM, Strickland DK, Bakillah A. The mammalian low-density lipoprotein receptor family. *Annu Rev Nutr*. 1999;19:141-172.
23. Argraves WS. Members of the low density lipoprotein receptor family control diverse physiological processes. *Front Biosci*. 2001;6:D406-D416.
24. Lee K, Shin Y, Cheng R, et al. Receptor heterodimerization as a novel mechanism for the regulation of Wnt/beta-catenin signaling. *J Cell Sci*. 2014;127:4857-4869.
25. Chen Q, Takahashi Y, Oka K, Ma JX. Functional differences of very-low-density lipoprotein receptor splice variants in regulating Wnt signaling. *Mol Cell Biol*. 2016;36:2645-2654.
26. Takahashi Y, Moiseyev G, Chen Y, Ma JX. Identification of conserved histidines and glutamic acid as key residues for isomerohydrolase activity of RPE65, an enzyme of the visual cycle in the retinal pigment epithelium. *FEBS Lett*. 2005;579:5414-5418.
27. Moiseyev G, Chen Y, Takahashi Y, Wu BX, Ma JX. RPE65 is the isomerohydrolase in the retinoid visual cycle. *Proc Natl Acad Sci USA*. 2005;102:12413-12418.
28. Lee K, Hu Y, Ding L, et al. Therapeutic potential of a monoclonal antibody blocking the Wnt pathway in diabetic retinopathy. *Diabetes*. 2012;61:2948-2957.
29. Qiu F, Ma X, Shin YH, et al. Pathogenic role of human C-reactive protein in diabetic retinopathy. *Clin Sci (Lond)*. 2020;134:1613-1629.
30. Gong Y, Li J, Sun Y, et al. Optimization of an image-guided laser-induced choroidal neovascularization model in mice. *PLoS One*. 2015;10:e0132643.
31. Qiu F, Meng T, Chen Q, et al. Fenofibrate-loaded biodegradable nanoparticles for the treatment of experimental diabetic retinopathy and neovascular age-related macular degeneration. *Mol Pharm*. 2019;16:1958-1970.
32. Yang Y, He X, Cheng R, et al. Diabetes-induced upregulation of kallistatin levels exacerbates diabetic nephropathy via RAS activation. *FASEB J*. 2020;34:8428-8441.
33. Wang N, Koutz CA, Anderson RE. A method for the isolation of retinal pigment epithelial cells from adult rats. *Invest Ophthalmol Vis Sci*. 1993;34:101-107.
34. Ma X, Takahashi Y, Wu W, et al. ADAM17 mediates ectodomain shedding of the soluble VLDL receptor fragment in the retinal epithelium. *J Biol Chem*. 2021;297:101185.
35. Meng XM, Nikolic-Paterson DJ, Lan HY. TGF-beta: the master regulator of fibrosis. *Nat Rev Nephrol*. 2016;12:325-338.
36. Yang X, Chung JY, Rai U, Esumi N. Cadherins in the retinal pigment epithelium (RPE) revisited: P-cadherin is the highly dominant cadherin expressed in human and mouse RPE in vivo. *PLoS One*. 2018;13:e0191279.
37. Han JW, Lyu J, Park YJ, Jang SY, Park TK. Wnt/beta-catenin signaling mediates regeneration of retinal pigment epithelium after laser photocoagulation in mouse eye. *Invest Ophthalmol Vis Sci*. 2015;56:8314-8324.
38. Luo X, Yang S, Liang J, et al. Choroidal pericytes promote subretinal fibrosis after experimental photocoagulation. *Dis Model Mech*. 2018;11:dmm032060.
39. Klapholz-Brown Z, Walmsley GG, Nusse YM, Nusse R, Brown PO. Transcriptional program induced by Wnt protein in human fibroblasts suggests mechanisms for cell cooperativity in defining tissue microenvironments. *PLoS One*. 2007;2:e945.
40. Masckauchan TN, Shawber CJ, Funahashi Y, Li CM, Kitajewski J. Wnt/beta-catenin signaling induces proliferation, survival and interleukin-8 in human endothelial cells. *Angiogenesis*. 2005;8:43-51.
41. Liu Y, Kanda A, Wu D, et al. Suppression of choroidal neovascularization and fibrosis by a novel RNAi therapeutic agent against (Pro)renin receptor. *Mol Ther Nucleic Acids*. 2019;17:113-125.
42. Masuzaki H, Jingami H, Matsuoka N, et al. Regulation of very-low-density lipoprotein receptor in hypertrophic rat heart. *Circ Res*. 1996;78:8-14.
43. Takahashi S, Sakai J, Fujino T, et al. The very low-density lipoprotein (VLDL) receptor: characterization and functions as a peripheral lipoprotein receptor. *J Atheroscler Thromb*. 2004;11:200-208.
44. Reddy SS, Connor TE, Weeber EJ, Rebeck W. Similarities and differences in structure, expression, and functions of VLDLR and ApoER2. *Mol Neurodegener*. 2011;6:30.
45. Sun Y, Lin Z, Liu CH, et al. Inflammatory signals from photoreceptor modulate pathological retinal angiogenesis via c-Fos. *J Exp Med*. 2017;214:1753-1767.
46. Xia CH, Lu E, Zeng J, Gong X. Deletion of LRP5 in VLDLR knockout mice inhibits retinal neovascularization. *PLoS One*. 2013;8:e75186.
47. Macosko EZ, Basu A, Satija R, et al. Highly parallel genome-wide expression profiling of individual cells using nanoliter droplets. *Cell*. 2015;161:1202-1214.

48. Ren S, Johnson BG, Kida Y, et al. LRP-6 is a coreceptor for multiple fibrogenic signaling pathways in pericytes and myofibroblasts that are inhibited by DKK-1. *Proc Natl Acad Sci USA*. 2013;110:1440-1445.
49. Ren Q, Chen J, Liu Y. LRP5 and LRP6 in Wnt signaling: similarity and divergence. *Front Cell Dev Biol*. 2021;9:670960.
50. Wang Z, Cheng R, Lee K, et al. Nanoparticle-mediated expression of a Wnt pathway inhibitor ameliorates ocular neovascularization. *Arterioscler Thromb Vasc Biol*. 2015;35:855-864.
51. Wu D, Kanda A, Liu Y, Kase S, Noda K, Ishida S. Galectin-1 promotes choroidal neovascularization and subretinal fibrosis mediated via epithelial-mesenchymal transition. *FASEB J*. 2019;33:2498-2513.
52. Saika S. TGFbeta pathobiology in the eye. *Lab Invest*. 2006;86:106-115.
53. Meyers EA, Kessler JA. TGF-beta family signaling in neural and neuronal differentiation, development, and function. *Cold Spring Harb Perspect Biol*. 2017;9:a022244.
54. Ma W, Silverman SM, Zhao L, et al. Absence of TGFbeta signaling in retinal microglia induces retinal degeneration and exacerbates choroidal neovascularization. *Elife*. 2019;8:42049.
55. Luo K. Signaling cross talk between TGF-beta/Smad and other signaling pathways. *Cold Spring Harb Perspect Biol*. 2017;9:a022137.

SUPPORTING INFORMATION

Additional supporting information may be found in the online version of the article at the publisher's website.

How to cite this article: Ma X, Takahashi Y, Wu W, et al. Soluble very low-density lipoprotein receptor (sVLDLR) inhibits fibrosis in neovascular age-related macular degeneration. *FASEB J*. 2021;35:e22058. doi:10.1096/fj.202101334R